

Columnar aerosol properties over oceans by combining surface and aircraft measurements: sensitivity analysis

Tianming Zhang and Howard R. Gordon

We report a sensitivity analysis for the algorithm presented by Gordon and Zhang [Appl. Opt. **34**, 5552 (1995)] for inverting the radiance exiting the top and bottom of the atmosphere to yield the aerosol-scattering phase function [$P(\Theta)$] and single-scattering albedo (ω_0). The study of the algorithm's sensitivity to radiometric calibration errors, mean-zero instrument noise, sea-surface roughness, the curvature of the Earth's atmosphere, the polarization of the light field, and incorrect assumptions regarding the vertical structure of the atmosphere, indicates that the retrieved ω_0 has excellent stability even for very large values (~ 2) of the aerosol optical thickness; however, the error in the retrieved $P(\Theta)$ strongly depends on the measurement error and on the assumptions made in the retrieval algorithm. The retrieved phase functions in the blue are usually poor compared with those in the near infrared.
© 1997 Optical Society of America

1. Introduction

In an earlier paper¹ we reported on an algorithm for retrieving columnar aerosol properties over oceans by inverting radiances exiting the boundary of the ocean-atmosphere system. We demonstrated that the algorithm has the potential to retrieve the aerosol scattering phase function [$P(\Theta)$] and single-scattering albedo (ω_0) accurately when combined with surface-based and high-altitude aircraft-based radiance measurements. However, all the inversions presented in Ref. 1 were based on the following idealizations and physical assumptions: (a) the radiometers measuring aerosol optical thickness (τ_a) as well as the upwelling and downwelling radiances have no calibration errors; (b) the instrumental noise in the measured radiances can be neglected; (c) the ocean surface is flat; (d) the Earth's curvature can be neglected; (e) the polarization of the light field can be neglected; and (f) the atmosphere contains two distinct layers, with a pure Rayleigh-scattering layer above a pure aerosol-scattering layer. In order to determine the range of applicability of the inversion

algorithm, it is necessary to investigate the algorithm's performance when these idealizations and assumptions are relaxed.

In this paper we begin by reviewing the algorithm in detail. Then we simulate pseudodata in which the various assumptions in the algorithm are violated one by one, e.g., noise is added to the pseudomeasurements, or pseudodata are simulated with the sea surface roughened by the wind. Finally, we assess the accuracy with which the algorithm can be expected to perform in realistic situations.

2. Inversion Algorithm

It is assumed that the normalized radiance ρ for the ocean-atmosphere system is measured at both the top (ρ_T) and bottom (ρ_B) of the atmosphere. The normalized radiance ρ is related to radiance L by

$$\rho = \pi L / F_0 \cos \theta_0, \quad (1)$$

where F_0 is the extraterrestrial solar irradiance and θ_0 is the solar zenith angle. We also assume that the aerosol optical thickness (τ_a) is measured at the sea surface by using a Sun photometer. The inversion algorithm is based on the fact that the normalized radiance distribution must carry information about the aerosol-scattering and absorption properties and therefore can be used to retrieve the aerosol-scattering phase function and the single-scattering albedo. If the atmosphere were optically thin, and

The authors are with the Department of Physics, University of Miami, Coral Gables, Florida 33124.

Received 10 June 1996; revised manuscript received 3 October 1996.

0003-6935/97/122650-13\$10.00/0

© 1997 Optical Society of America

in the absence of molecular scattering, ρ at the boundaries would be proportional to $\omega_0\tau_a P(\Theta)$ evaluated at the appropriate single-scattering angle Θ . Thus, the measurement of ρ_T , ρ_B , and τ_a would yield $\omega_0 P(\Theta)$. This simple analysis is complicated by multiple scattering, which must be considered in ρ_B for τ_a as small as 0.05, e.g., a single-scattering computation of ρ_B can be in error by as much as a factor of ~ 2 in the almucantar of the Sun for $\tau_a = 0.05$ and $\theta_0 = 60^\circ$.² An algorithm that utilizes downwelling radiances ρ_B to retrieve ω_0 and $P(\Theta)$ for a partial range of Θ ($0 < \Theta < \pi/2 + \theta_0$) has already been described by Wang and Gordon.³ In this Section we provide the details of how ω_0 and $P(\Theta)$ for the full range of Θ can be retrieved when the upwelling radiances ρ_T are added. We note that ρ_T , ρ_B , ω_0 , τ_a , and $P(\Theta)$ are all functions of wavelength (λ); however, in what follows, for economy, the dependence on λ will be suppressed.

Given a guess for $\omega_0 P(\Theta)$ and the measured value of τ_a , the radiative transfer equation (RTE) can be solved for ρ_T and ρ_B . A comparison of these with their measured counterparts will indicate that $\omega_0 P(\Theta)$ must be changed to bring the measured and computed values into agreement. The key to the algorithm is the systematic variation of $\omega_0 P(\Theta)$ to force the computed ρ 's to agree with the measured ones. This is accomplished as follows.

We define a spherical coordinate system with the z axis pointing down to the Earth. Let the Sun's rays have a polar angle θ_0 and an azimuthal angle $\phi_0 = 0^\circ$. In this coordinate system, photons contributing to ρ_B have $\theta < 90^\circ$, whereas those contributing to ρ_T have $\theta > 90^\circ$. As it has been found from lidar profiles⁴ that typically most of the aerosols are confined to a layer of ~ 2 km thickness near the sea surface, i.e., most of the molecular scattering originates above the aerosols, we simplify the atmosphere and model it as a two-layer system with Rayleigh scattering above the aerosols. Also, the atmosphere is assumed to be bounded by a flat, Fresnel-reflecting ocean. For the ocean-atmosphere system, the total reflectance at the top of the atmosphere (TOA) is given by

$$\rho_T = \rho_r + \rho_a + \rho_{ra} + t\rho_w, \quad (2)$$

where ρ_r and ρ_a are the reflectances resulting from, respectively, multiple scattering by air molecules (Rayleigh scattering) and aerosols in the atmosphere, ρ_{ra} is the interaction term between molecular and aerosol scattering, and $t\rho_w$ is the water-leaving radiance propagating to the TOA. Note that in Eq. (2), the Sun glitter contribution (direct solar radiation specularly reflected from the ocean surface) to the total reflectance has been ignored, because when ρ_T is measured, the specular image of the Sun is to be avoided.

Assuming that $t\rho_w$ is known, e.g., from ship-based measurements made simultaneously with the sky radiance measurements, we can find

$$\rho_a + \rho_{ra} = \rho_T - \rho_r - t\rho_w. \quad (3)$$

The value of the left-hand side of Eq. (3) depends on the optical properties of the aerosols; we assume that

it is proportional to the single scattering by aerosols ρ_{as} , i.e.,

$$\rho_T - \rho_r - t\rho_w \propto \rho_{as}. \quad (4)$$

Here ρ_{as} is composed of three parts: (i) direct single scattering without surface reflection involved, (ii) reflection of the direct solar beam from a flat sea surface followed by single scattering in the atmosphere, and (iii) single scattering toward the flat sea surface followed by reflection from the surface. Usually, (ii) and (iii) are much smaller than (i). If we neglect (ii) and (iii) and express (i) analytically by using aerosol optical properties, we have at the TOA

$$\rho_{as} = -\frac{\omega_0\tau_a P(\Theta)}{4 \cos \theta \cos \theta_0}, \quad \theta > 90^\circ, \quad (5)$$

where θ and ϕ define the polar and azimuth angles of photons traveling in the viewing direction, and Θ is the scattering angle given by

$$\cos \Theta = \cos \theta_0 \cos \theta + \sin \theta_0 \sin \theta \cos(\phi - \phi_0). \quad (6)$$

Now if we assume a function for $\omega_0 P(\Theta)$, e.g., a Henyey-Greenstein phase function,⁵ the upwelling reflectance of the two-layer atmosphere-ocean system can be calculated exactly by solving the RTE. Also, ρ_r can be determined easily by solving the RTE for a uniform layer of molecular scattering above a Fresnel-reflecting flat ocean surface. Let the superscript (m) denote the measured value, and let the superscript (c) denote the value calculated by solving the RTE by using an assumed $\omega_0 P(\Theta)$, i.e., by using $[\omega_0 P(\Theta)]^{(c)}$. We use the single-scattering approximation to estimate the error in $[\omega_0 P(\Theta)]^{(c)}$. Letting $[\omega_0 P(\Theta)]^{(t)}$ be the true scattering function, we have

$$\rho_T^{(m)} - \rho_r^{(c)} - t\rho_w^{(m)} \propto -\frac{\tau_a[\omega_0 P(\Theta)]^{(t)}}{4 \cos \theta \cos \theta_0}, \quad (7)$$

$$\rho_T^{(c)} - \rho_r^{(c)} - t\rho_w^{(m)} \propto -\frac{\tau_a[\omega_0 P(\Theta)]^{(c)}}{4 \cos \theta \cos \theta_0}, \quad (8)$$

$$\frac{\rho_T^{(c)} - \rho_T^{(m)}}{\rho_T^{(m)} - \rho_r^{(c)} - t\rho_w^{(m)}} = \frac{\Delta[\omega_0 P(\Theta)]}{[\omega_0 P(\Theta)]^{(t)}}, \quad (9)$$

where

$$\Delta[\omega_0 P(\Theta)] = [\omega_0 P(\Theta)]^{(c)} - [\omega_0 P(\Theta)]^{(t)}. \quad (10)$$

From Eq. (9) we find that the error in $\omega_0 P(\Theta)$ is

$$\Delta[\omega_0 P(\Theta)] = \frac{\rho_T^{(c)} - \rho_T^{(m)}}{\rho_T^{(m)} - \rho_r^{(c)} - t\rho_w^{(m)}} [\omega_0 P(\Theta)]^{(t)}. \quad (11)$$

Because $[\omega_0 P(\Theta)]^{(t)}$ is unknown we estimate it by $[\omega_0 P(\Theta)]^{(c)}$, and then Eq. (11) can be used to estimate $\Delta[\omega_0 P(\Theta)]$ for values of Θ provided by Eq. (6). {An anonymous reviewer correctly pointed out to us that this assumption is unnecessary. If the denominator of Eq. (9), i.e., relation (7), is replaced by relation (8), then in Eq. (11) $\rho_T^{(m)}$ in the denominator is replaced by $\rho_T^{(c)}$, and $[\omega_0 P(\Theta)]^{(t)}$ is replaced by $[\omega_0 P(\Theta)]^{(c)}$. In

this case, all the quantities in the equation are known. We applied this in place of Eq. (11) for a sample of the computations presented below in Figs. 4(d), 5(c), 5(d), and 6(b). The results were virtually identical to those obtained by using Eq. (11).} The new value of $\omega_0 P(\Theta)$ is taken to be

$$[\omega_0 P(\Theta)]_{\text{new}} = [\omega_0 P(\Theta)]_{\text{old}} - C \Delta[\omega_0 P(\Theta)], \quad (12)$$

where C is a constant between 0 and 1, and is usually taken to be ~ 0.5 . For radiances measured at the sea surface, the procedure for estimating $\Delta[\omega_0 P(\Theta)]$ is similar to the above, except that the contribution from Rayleigh scattering has to propagate through the aerosol layer, and therefore the ρ_r 's in the above equations should be replaced by $\rho_r \exp(-\tau_a/\cos \theta)$. Also, $t\rho_w$ is left out, and ρ_B replaces ρ_T .

The new value of $\omega_0 P(\Theta)$ is then inserted into the RTE to solve for $\rho_T^{(c)}$ and $\rho_B^{(c)}$, and the above process is repeated until convergence is achieved. Finally, after $\omega_0 P(\Theta)$ has been retrieved for $0 < \Theta < \pi$ from both downwelling and upwelling radiances, ω_0 and $P(\Theta)$ can be obtained by the normalization relation for the phase function, i.e.,

$$\omega_0 = \frac{1}{2} \int_0^\pi [\omega_0 P(\Theta)] \sin \Theta d\Theta, \quad (13)$$

$$P(\Theta) = \frac{1}{\omega_0} [\omega_0 P(\Theta)]. \quad (14)$$

Note that the aerosol phase function $P(\Theta)$ is normalized to 4π .

To carry out the inversion one must have simultaneous measurements of direct solar extinction (for τ_a) and diffuse radiances [for $\rho_B^{(m)}$ and $\rho_T^{(m)}$]. In our simulation, we assume that the radiances are measured as follows.

(1) Surface almuantar: first make the detector view at the Sun, then keep its viewing angle $\theta = \theta_0$, and then move the detector from $\phi = 0^\circ$ to $\phi = 360^\circ$. Because of symmetry, actually only the radiances with ϕ from 0° to 180° are used. These almuantar radiances will be utilized to retrieve the phase function $P(\Theta)$ for scattering angle $0 < \Theta < 2\theta_0$.

(2) Downwelling principal plane: this set of radiances has propagating directions with $\phi = 180^\circ$ and $\theta_0 < \theta < 90^\circ$. They correspond to the scattering angle of $2\theta_0 < \Theta < \theta_0 + 90^\circ$.

(3) Upwelling principal plane: this part of the radiance data is assumed to be measured by aircraft or satellite. The azimuthal angles are $\phi = 180^\circ$, $\phi = 0^\circ$, or both. Depending on θ_0 , proper θ values should be selected so that they will cover the rest of the scattering angle range, i.e., $\theta_0 + 90^\circ < \Theta < 180^\circ$, and avoid the specular image of the Sun.

Note that the above three sets of radiance data will cover the whole scattering angle range (from 0° to 180°) but *with no overlap*. We have found that this is important, because the redundant data (ρ_T and ρ_B

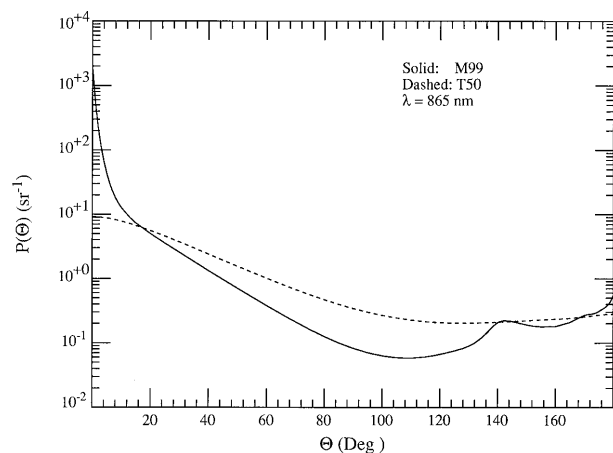


Fig. 1. Scattering phase functions for the Shettle and Fenn models M99 and T50.

data corresponding to the same single-scattering angle Θ), which result from overlap, can possess significantly different multiple-scattering effects and therefore slow or stop the convergence of the algorithm. However, we have not found it necessary to take any special action at the boundaries between regions that may have significantly different multiple-scattering effects.

3. Sensitivity Analysis

To test the algorithm's sensitivity to the various assumptions employed, we used the Shettle and Fenn⁶ tropospheric aerosol model with a relative humidity of 50% (T50) and their maritime model with a relative humidity of 99% (M99). The scattering phase functions at 865 nm for these models are shown in Fig. 1. The M99 phase function is the most sharply peaked in the forward direction and has the most structure near the rainbow angle ($\Theta \sim 140^\circ$) of any of the Shettle and Fenn models, and it provides a severe test of the retrieval algorithm. Figures 2 and 3 show how well the product of the single-scattering albedo and the phase function can be retrieved for $\theta_0 = 60^\circ$ and $\lambda = 865$ nm when all the assumptions in the algorithm are true. Even when τ_a is as large as 2.0, the maximum error in $\omega_0 P(\Theta)$ is $\sim 3.5\%$ near the rainbow angle and $< 1\%$ elsewhere for M99, and the maximum error in $\omega_0 P(\Theta)$ is $< 1.5\%$ for T50 at all values of Θ . For ω_0 , the error is always $< 0.1\%$ in all four cases.

Now we investigate the stability of the retrieval algorithm under the influence of radiometric calibration errors, instrumental noise, sea-surface roughness, the Earth's curvature, light-field polarization, and variations in the vertical structure of atmosphere. In all cases, the solar zenith angle is 60° .

A. Sensitivity to Error in the τ_a Measurement

To determine the algorithm's sensitivity to error in the τ_a measurement, we carried out simulations by adding $\pm 5\%$ error to the value of τ_a used to solve the RTE in the retrieval process. Figure 4 presents the

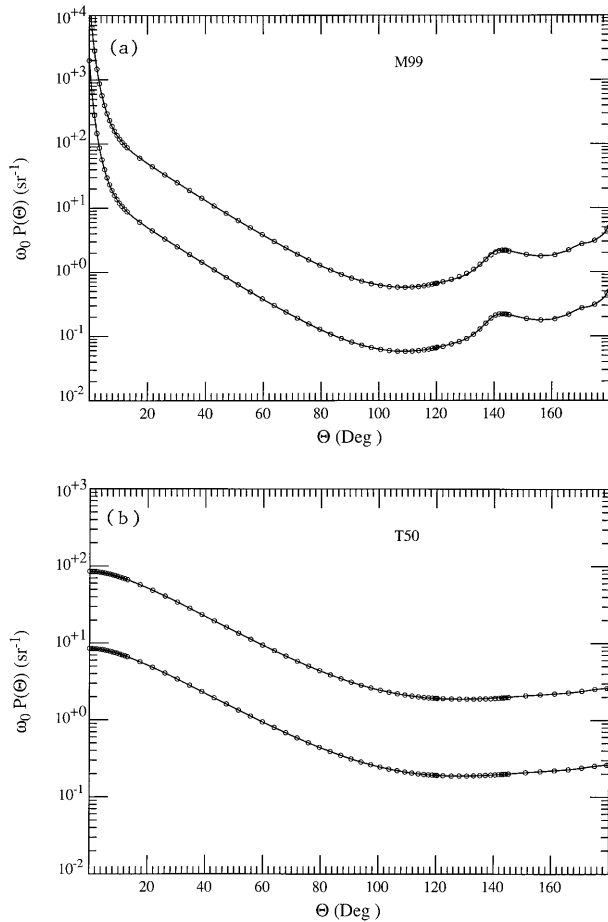


Fig. 2. Comparison between the true $\omega_0 P_a(\Theta)$ (solid curves) and the retrieved $\omega_0 P_a(\Theta)$ (circles) for $\lambda = 865$ nm and $\theta_0 = 60^\circ$: (a) M99, (b) T50. Lower curves, $\tau_a = 0.2$; upper curves, $\tau_a = 2.0$ (values for $\tau_a = 2.0$ are $\times 10$).

error in the retrieved $\omega_0 P(\Theta)$ in this situation for $\lambda = 865$ nm. When $\tau_a = 0.2$, which is somewhat larger than typical values over the ocean,⁷⁻⁹ a $\pm 5\%$ error in τ_a results in an error with a similar magnitude in the retrieved $\omega_0 P(\Theta)$ for most scattering angle ranges and an approximately $\mp 3\%$ error in ω_0 . This agrees with the single-scattering approximation [Eq. (5)], for which the error in ω_0 would be $\mp 5\%$. For $\tau_a = 2.0$, because of the strong multiple scattering, the sensitivity to error in τ_a increases, with the maximum error in $\omega_0 P(\Theta)$ being $\sim 15\%$; however, it is interesting to note that the multiple scattering helps to reduce the error in the retrieved ω_0 induced by the error in τ_a . When the error in τ_a is $\pm 5\%$, the error in the retrieved ω_0 is only approximately $\pm 0.5\%$ for T50 and $< 0.1\%$ for M99. So, the upper limit to the error in the retrieved ω_0 is the error in measured τ_a , and it decreases as τ_a increases. In contrast, for small τ_a , the phase function error is smaller than the error in τ_a , but it increases significantly as τ_a increases.

B. Sensitivity to Error in the Measured ρ_B and ρ_T

Because simultaneous radiance measurements at the TOA and at the sea surface are required, we have to consider the calibration errors of two radiometers—

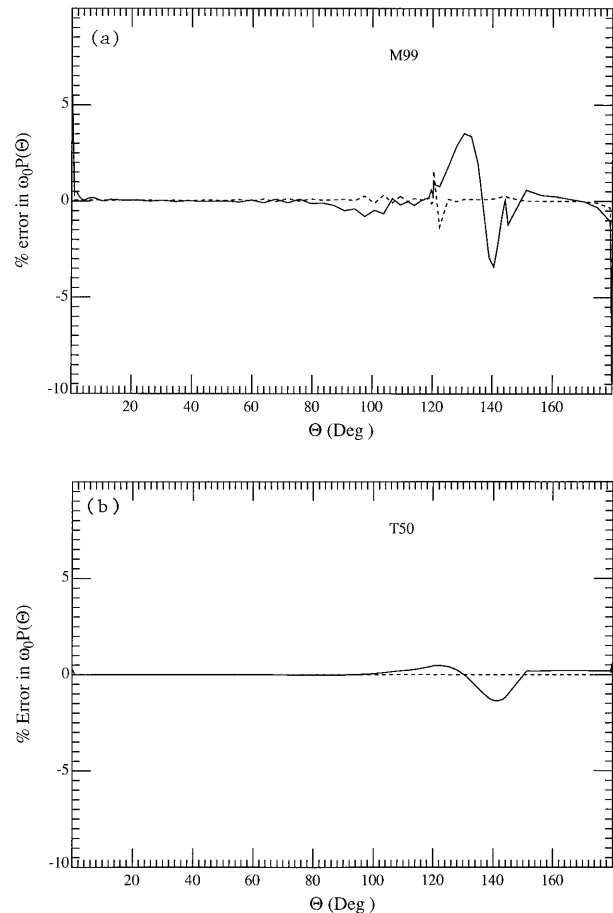


Fig. 3. Percent error in $\omega_0 P_a(\Theta)$ for $\tau_a = 0.2$ (dashed curves) and $\tau_a = 2.0$ (solid curves) for $\lambda = 865$ nm and $\theta_0 = 60^\circ$: (a) M99, (b) T50.

one measuring upwelling radiances at the TOA and the other measuring downwelling radiances at the surface. Therefore, two sets of simulations have been carried out to study the algorithm's sensitivity to the calibration errors: one set corresponds to the case in which the two sensors both have $+5\%$ or -5% calibration errors, and the other set corresponds to the case in which one sensor has $+5\%$ error and the other has -5% error. Such retrievals for the M99 aerosol at $\lambda = 865$ nm are provided in Fig. 5. Figures 5(a) and 5(b) are for $\tau_a = 0.2$, and Fig. 5(c) and 5(d) are for $\tau_a = 2.0$. The first impression is that, in each of the four figures, the solid curve and the dashed curve are roughly symmetric with respect to the dotted line (the error-free line).

For $\tau_a = 0.2$, because single scattering contributes significantly to the total radiance, as expected from Eq. (5), an error in the measured radiance will result in an error of similar value in the retrieved $\omega_0 P(\Theta)$. From Figs. 5(a) and 5(b) we can see that this is true for most scattering angles, where the multiple scattering is weak. However, for the case in which ρ_B and ρ_T contain errors with a different sign, the error in the retrieved $\omega_0 P(\Theta)$ for $150^\circ < \Theta < 180^\circ$, which is inverted from upwelling radiances, for which multi-

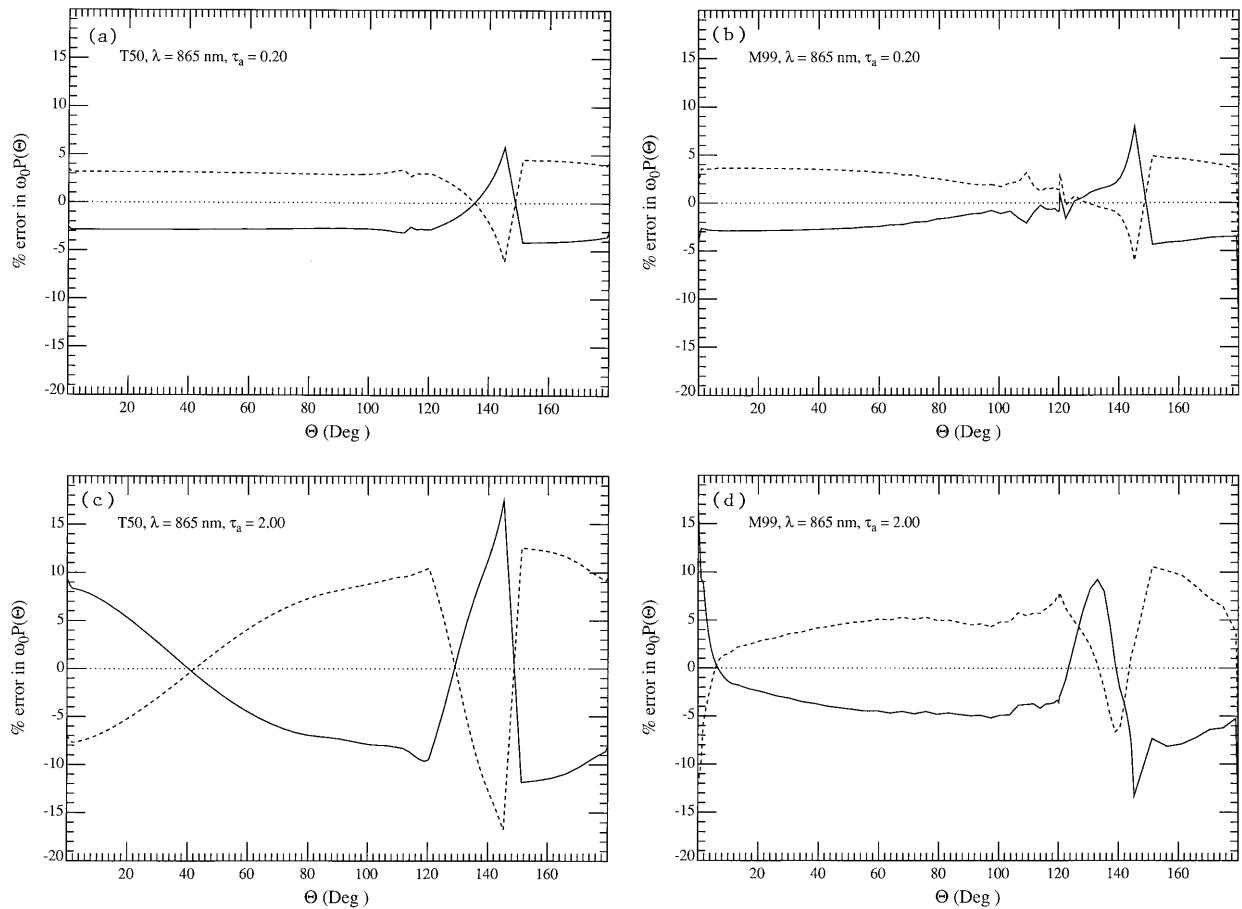


Fig. 4. Percent error in the retrieved $\omega_0 P(\Theta)$ when the measured τ_a has a +5% error (solid curves) and a -5% error (dashed curves) with $\theta_0 = 60^\circ$ and $\lambda = 865$ nm: (a) T50, true $\tau_a = 0.2$; (b) M99, true $\tau_a = 0.2$; (c) T50, true $\tau_a = 2.0$; (d) M99, true $\tau_a = 2.0$.

ple scattering is weak, is much larger than $\pm 5\%$ in $\rho_T^{(m)}$ (the error being approximately $\pm 15\%$). In the single-scattering limit, it is easy to show that a positive (negative) error in $\omega_0 P(\Theta)$ for $0^\circ < \Theta < 150^\circ$ tends to enlarge the negative (positive) error in $\omega_0 P(\Theta)$ for $150^\circ < \Theta < 180^\circ$ as a result of sea-surface interaction. Figure 5 shows that this effect is enhanced by multiple scattering. For the retrieved ω_0 , the error is approximately $\pm 4\%$ when the measured $\rho_B^{(m)}$ has $\pm 5\%$ error. The retrieved ω_0 is not influenced significantly by the error in $\rho_T^{(m)}$ because most of the integral in Eq. (13) comes from the forward direction.

For $\tau_a = 2.0$, because of the strong multiple-scattering effect, the error in the retrieved $\omega_0 P(\Theta)$ is much larger than that for $\tau_a = 0.2$, with the maximum being $\sim 30\%$. However, the ω_0 can still be retrieved accurately. When the error in $\rho_B^{(m)}$ is $\pm 5\%$, the error in the retrieved ω_0 is only approximately $\pm 1\%$. Again, we see that the retrieved ω_0 has better stability when τ_a is larger.

The above simulations are all for $\lambda = 865$ nm. Some similar simulations have been carried out for $\lambda = 412$ nm. The results are significantly poorer than those at $\lambda = 865$ nm, because for $\lambda = 412$ nm much more of the total radiance comes from Rayleigh scattering. In the retrieval algorithm, the Rayleigh ra-

diance is calculated exactly. Therefore, an error in the total radiance is equivalent to a much larger error in the aerosol contribution, which will result in a larger error in the retrieval. This shows that for retrievals in the blue with accuracies similar to those in the near infrared to be carried out, more accurate measurements of ρ_T and ρ_B will be required.

C. Sensitivity to Instrumental Noise

In reality, the measured radiances also contain errors that are due to the instrumental noise. Figure 6 provides simulations for M99 aerosol with $\theta_0 = 60^\circ$ for the situation in which $\rho_B^{(m)}$ and $\rho_T^{(m)}$ have been augmented by mean-zero Gaussian noise with a standard deviation of 0.5%, corresponding to a signal-to-noise ratio of 200. Figures 6(a) and 6(b) are for $\lambda = 865$ nm with $\tau_a = 0.2$ and $\tau_a = 2.0$, respectively. As we can see, the noise in $\rho_B^{(m)}$ and $\rho_T^{(m)}$ results in a noisy phase function, and when τ_a increases, the multiple scattering exaggerates the noise in the retrieved $\omega_0 P(\Theta)$. The maximum error in $\omega_0 P(\Theta)$ is $\sim 3\%$ for $\tau_a = 0.2$ and $\sim 40\%$ for $\tau_a = 2.0$. However, ω_0 is not affected as much as the phase function; the error is only approximately -0.2% for $\tau_a = 0.2$, and approximately 0.1% for $\tau_a = 2.0$.

Figures 6(c) and 6(d) provide such retrievals at $\lambda = 412$ nm for $\tau_a = 0.2$ and $\tau_a = 2.0$, respectively. As a

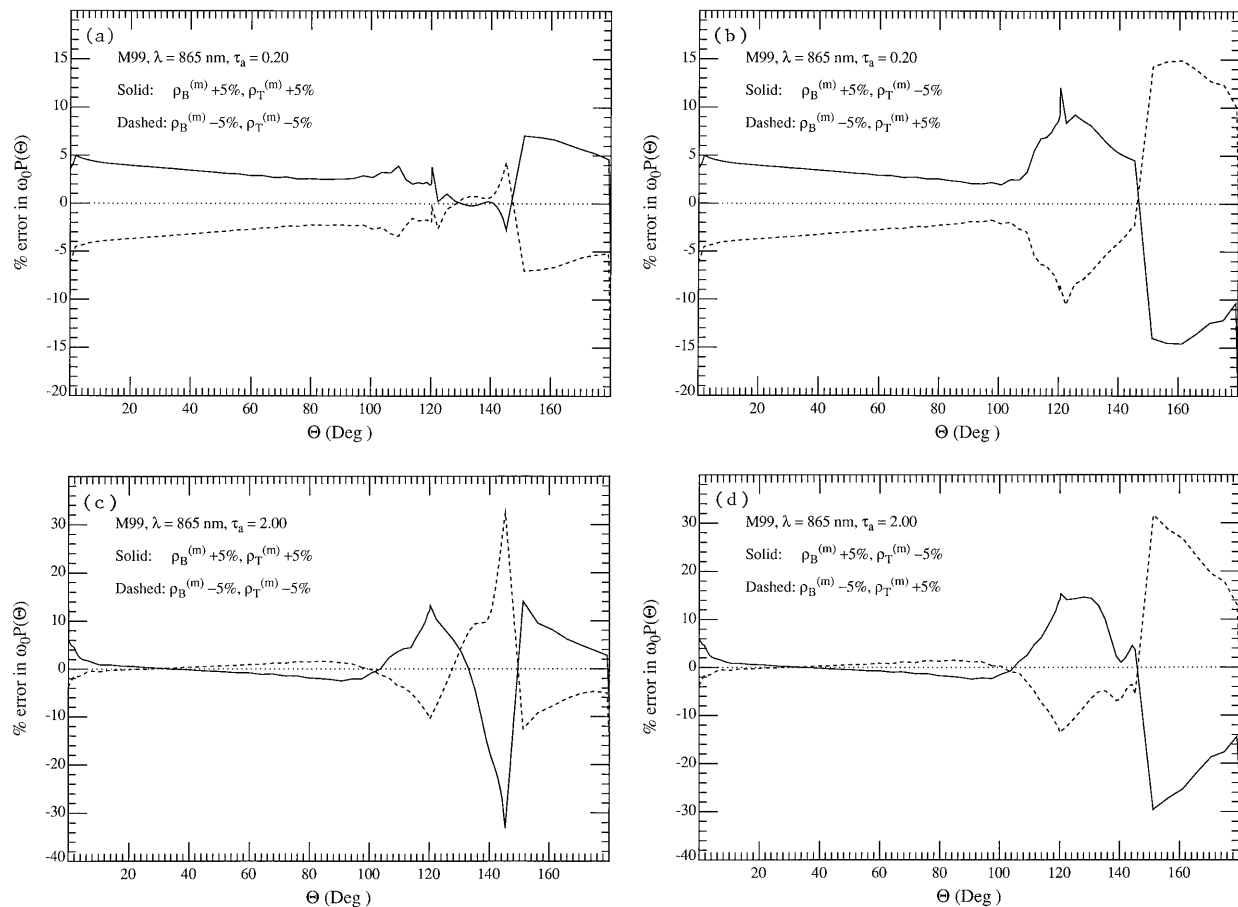


Fig. 5. Percent error in the retrieved $\omega_0 P(\Theta)$ when $\rho_B^{(m)}$ and $\rho_T^{(m)}$ contain a +5% or -5% error for $\theta_0 = 60^\circ$ and $\lambda = 865$ nm: (a), (b) true $\tau_a = 0.2$; (c), (d) true $\tau_a = 2.0$. Note the change of scale between (a) and (b) and (c) and (d).

result of the increased Rayleigh-scattering contribution, the retrievals of the phase function are degraded in both figures. The maximum error in $\omega_0 P(\Theta)$ is $\sim 100\%$ for $\tau_a = 0.2$ and a little larger than 100% for $\tau_a = 2.0$. However, the retrieved ω_0 is excellent, with the error being $< 0.1\%$ for the conditions that hold in Fig. 6(c) and $\sim 1\%$ for those in Fig. 6(d).

The easiest way of understanding the effect of noise seen in Fig. 6 is to consider the reverse problem, i.e., the addition of mean-zero noise to $\omega_0 P(\Theta)$, which will not alter the value of ω_0 . Then the single-scattering contributions to ρ_T and ρ_B will completely reflect the noise, whereas the multiple-scattering contributions, being integrals over the scattering angle of the product of two or more phase functions evaluated at different Θ 's, will not. Thus, as τ_a increases, the effect of noise in $\omega_0 P(\Theta)$ will be less and less reflected in variations in ρ_T and ρ_B . Conversely, as τ_a increases, variations (noise) in ρ_T and ρ_B will be reflected in larger and larger variations in the retrieved $\omega_0 P(\Theta)$; however, the retrieved value of ω_0 should be relatively independent of the noise in the measurements.

D. Influence of Sea Surface Roughness

Our retrieval algorithm assumes a flat ocean surface. However, the ocean surface is almost always ruffled by wind. To study how the sea-surface roughness

will affect the retrieval, we apply the model of the rough sea surface developed by Cox and Munk.¹⁰ In this model the distribution of surface slopes is a Gaussian function. In the simulations presented here, the pseudoradiance data were created by assuming a rough sea surface corresponding to an omnidirectional wind with a speed of 7.5 m/s; however, when the retrievals were carried out, the sea surface was assumed to be flat. Figure 7 presents retrievals: Figs. 7(a) and 7(b) are for $\lambda = 865$ nm, and $\tau_a = 0.2$ and $\tau_a = 2.0$, respectively. We can see that, in both figures, the errors in the retrieved $\omega_0 P(\Theta)$ are within 5% except for $120^\circ < \Theta < 150^\circ$, where the large errors occur as a result of strong multiple-scattering effects. The errors in ω_0 are $\sim 0.1\%$ for both cases. Figure 7(c) is for $\tau_a = 2.0$ and $\lambda = 412$ nm. The retrieval result is poorer than that at $\lambda = 865$ nm, with the maximum error in $\omega_0 P(\Theta)$ being $\sim 70\%$ and the error in ω_0 being $\sim 1\%$.

Note that the large errors usually appear within the range $120^\circ < \Theta < 146^\circ$, where the phase functions are retrieved from downwelling principal plane radiance pseudodata with $60^\circ < \theta < 86^\circ$. This happens because these downwelling principal plane pseudodata are more influenced by multiple scattering. Much better results have been obtained by carrying out the simulations by using upwelling

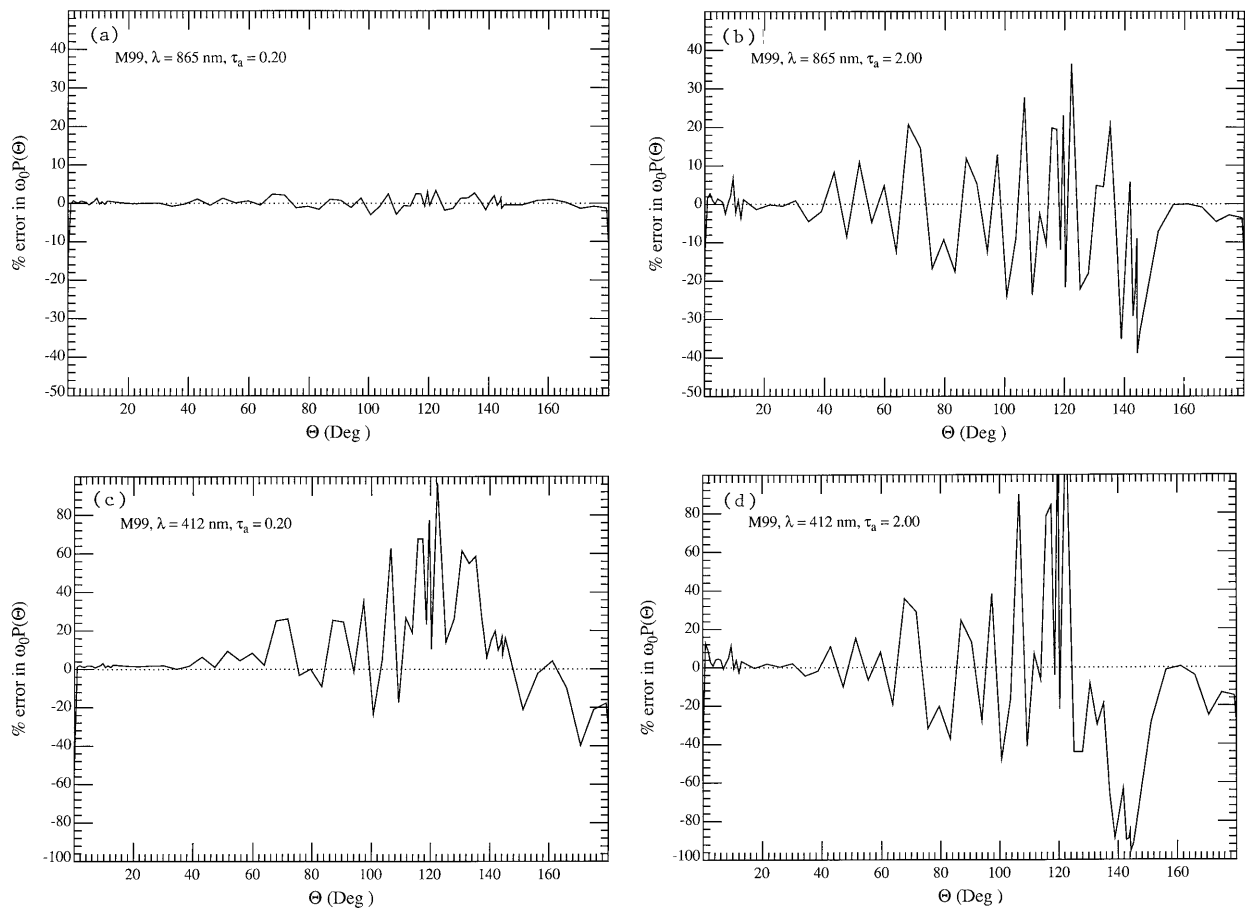


Fig. 6. Percent error in the retrieved $\omega_0 P(\Theta)$ for M99 aerosol when $\rho_B^{(m)}$ and $\rho_T^{(m)}$ contain a $\pm 0.5\%$ mean-zero Gaussian noise when $\theta_0 = 60^\circ$: (a) $\lambda = 865$ nm, $\tau_a = 0.2$; (b) $\lambda = 865$ nm, $\tau_a = 2.0$; (c) $\lambda = 412$ nm, $\tau_a = 0.2$; (d) $\lambda = 412$ nm, $\tau_a = 2.0$. Note the change of scale between $\lambda = 412$ and 865 nm.

principal plane pseudodata with $150^\circ < \theta < 180^\circ$ and $\phi = 180^\circ$ to replace the downwelling principal plane pseudodata. Figure 7(d) is one example of such retrieval. Everything is the same as in Fig. 7(c) except that the downwelling principal plane data have been replaced by upwelling radiance data. Comparing Fig. 7(d) with Fig. 7(c), we can see that the error in $\omega_0 P(\Theta)$ presented by Fig. 7(d) has been significantly reduced, with the maximum being $\sim 20\%$.

E. Neglect of the Earth's Curvature

So far, simulations have been carried out under the assumption that the atmosphere is a plane-parallel medium, i.e., the Earth's curvature has been ignored. To illustrate the performance of the algorithm when the Earth's curvature is taken into account, we have computed the pseudodata $\rho_B^{(m)}$ and $\rho_T^{(m)}$ by a backward Monte Carlo radiative transfer code,¹¹ in which the atmosphere is modeled as a two-layer spherical shell medium with aerosols confined between 0 and 2 km and Rayleigh scattering confined between 2 and 20 km. In the retrieval algorithm, the atmosphere is still assumed to be plane parallel. Figures 8(a) and 8(b) provide the error in the retrieved $\omega_0 P(\Theta)$ for the M99 aerosol at $\lambda = 865$ nm. The oscillations in these figures are due to statistical fluctuations in the

Monte Carlo calculations, which have the effect of adding mean-zero noise to the pseudodata. When $\tau_a = 2.0$, these fluctuations result in significant variations in the retrieved $\omega_0 P(\Theta)$. As we can see, the maximum error in $\omega_0 P(\Theta)$ is $\sim 5\%$ in Fig. 8(a) and $\sim 25\%$ in Fig. 8(b). Figure 8(a) also shows that when $\tau_a = 0.2$ there is a systematic negative error in $\omega_0 P(\Theta)$ for $\Theta < 150^\circ$. This is the result of the fact that in the solar almucantar the plane-parallel model progressively overestimates ρ_B as ϕ increases, i.e., smaller values of $\omega_0 P(\Theta)$ are required in the plane-parallel model to reproduce the measured ρ_B . This systematic error leads to an approximately -0.4% error in ω_0 for $\tau_a = 0.2$. For $\tau_a = 2.0$ the error in ω_0 is reduced to $\sim 0.1\%$. These results suggest that ignoring the Earth's curvature does not lead to an extraordinarily large error in $\omega_0 P(\Theta)$. We expected that the error might be reduced by replacing the ρ_B principal plane pseudodata, which are more influenced by the Earth's curvature, by ρ_T pseudodata; however, there was little or no improvement when this was effected.

F. Neglect of Light-Field Polarization in the Retrieval Algorithm

Unpolarized light (e.g., the solar beam at the top of the atmosphere) generally will become partially po-

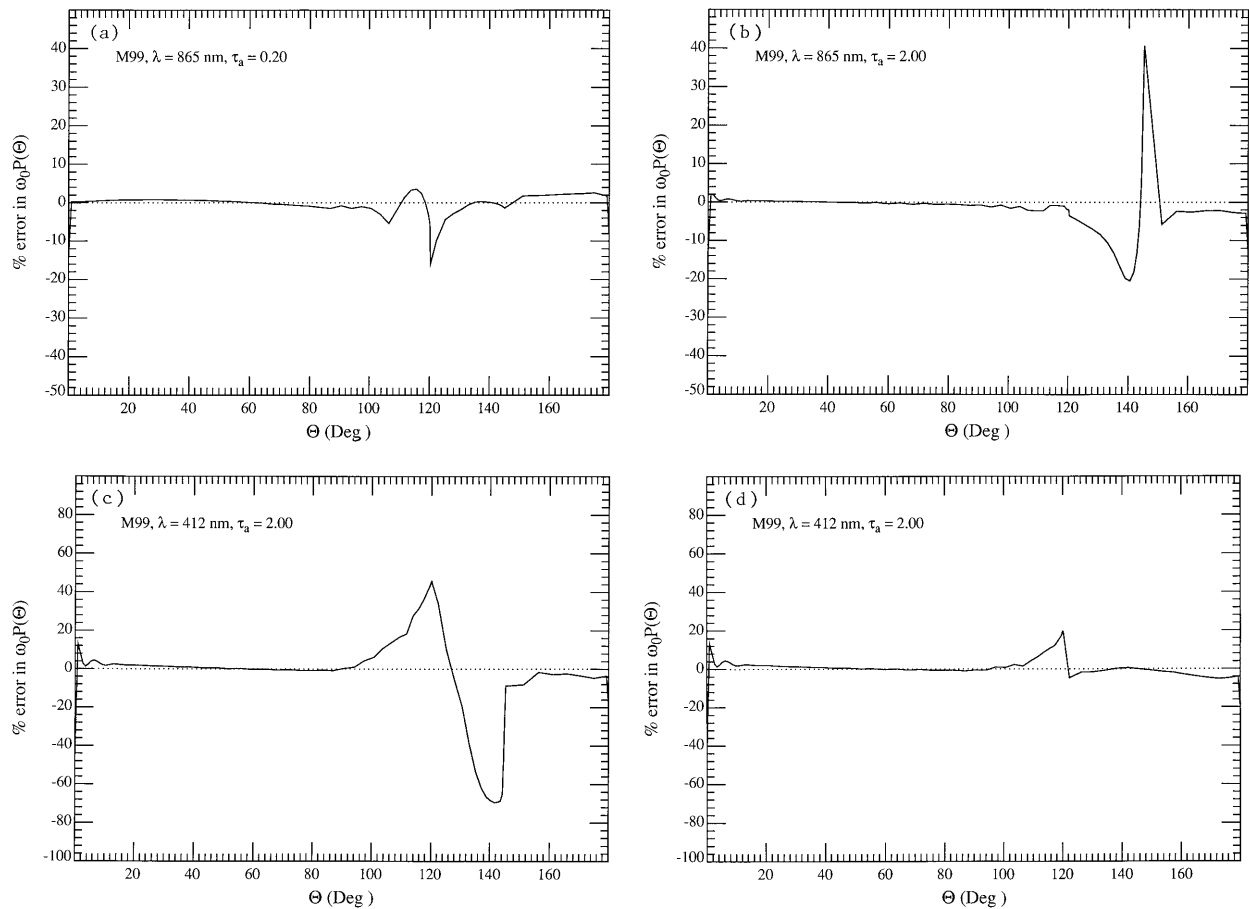


Fig. 7. Percent error in the retrieved $\omega_0 P(\Theta)$ for M99 aerosol when $\rho_B^{(m)}$ and $\rho_T^{(m)}$ are computed for a rough sea surface with $W = 7.5$ m/s and $\theta_0 = 60^\circ$: (a) $\lambda = 865$ nm, $\tau_a = 0.2$; (b) $\lambda = 865$ nm, $\tau_a = 2.0$; (c) $\lambda = 412$ nm, $\tau_a = 2.0$; (d) $\lambda = 412$ nm, $\tau_a = 2.0$, but the downwelling principal plane data were replaced by upwelling data. Note the change of scale between (a) and (b) and (c) and (d).

larized after being scattered in the atmosphere or reflected from the ocean surface. Therefore, polarization effects should be considered when the radiative transfer processes in an ocean-atmosphere system are dealt with. In our algorithm, we have been using scalar radiative transfer theory to calculate the radiance exiting the ocean-atmosphere system. This will lead to an error of a few percent in the calculated radiance.^{12,13} To investigate the error in the retrieval induced by ignoring polarization, we carried out simulations with polarization included in $\rho_t^{(m)}$ (the vector radiative transfer theory).^{14,15} However, because much of the polarization effect comes from Rayleigh scattering, in order to reduce the errors in the retrieved aerosol properties caused by the Rayleigh-scattering polarization effect, $\rho_T^{(m)}$ and $\rho_B^{(m)}$ have been modified as $\rho_T^{(m)} - [\rho_r^{(v)} - \rho_r^{(s)}]$ and $\rho_B^{(m)} - [\rho_r^{(v)} - \rho_r^{(s)}]\exp(-\tau_a/\cos \theta)$ before being inserted into the retrieval algorithm, where $\rho_r^{(v)}$ and $\rho_r^{(s)}$ are the radiances calculated for a plane-parallel Rayleigh-scattering layer above a flat ocean surface by using vector and scalar transfer theories respectively. Thus, that part of the polarization effect that is due to Rayleigh scattering was approximately accounted for in the inversion algorithm. Simulated retrievals applying this scheme for the T50 aerosol

with $\theta_0 = 60^\circ$ and $\lambda = 865$ nm are provided in Fig. 9. Figure 9(a) is for $\tau_a = 0.2$. We can see that when τ_a is small, the error in $\omega_0 P(\Theta)$ induced by ignoring polarization is usually $< 6\%$. It is easy to show through a single-scattering analysis that the error in $\omega_0 P(\Theta)$ is primarily caused by the difference between the single-scattering components that involve surface reflection, when light polarization is included and neglected. Figure 9(b) is for $\tau_a = 2.0$. As a result of strong multiple-scattering effects, the error in $\omega_0 P(\Theta)$ is much larger, with the maximum being $\sim 30\%$. Figure 9(c) presents a retrieval similar to Figure 9(b) but uses more upwelling principal plane data to replace the downwelling principal plane data. As we can see, the error in $\omega_0 P(\Theta)$ has been greatly reduced, with the maximum being $\sim 6\%$. The retrieved ω_0 are all excellent, with the error being $\sim 0.1\%$.

G. Variations in the Vertical Structure of the Atmosphere
The simulations described thus far have been carried out under the idealization that the atmosphere is composed of a layer of *pure* Rayleigh scattering above a layer of *pure* aerosol scattering. It has further been assumed that the correct vertical structure is used in the inversion algorithm. We note that, in reality, Rayleigh scattering and aerosol scattering

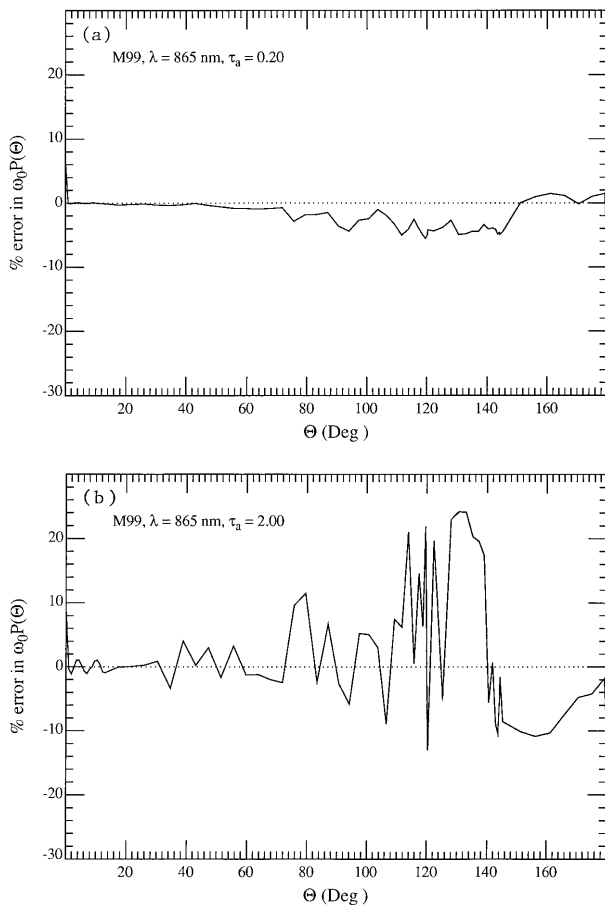


Fig. 8. Percent error in the retrieved $\omega_0 P(\Theta)$ for M99 aerosol when $\rho_B^{(m)}$ and $\rho_T^{(m)}$ are computed by assuming a spherical shell atmosphere, with $\theta_0 = 60^\circ$ and $\lambda = 865$ nm: (a) $\tau_a = 0.2$; (b) $\tau_a = 2.0$.

are always mixed in the atmosphere and the vertical structure of the aerosol may not be known. Here we investigate the algorithm's performance when Rayleigh scattering and aerosol scattering are mixed, and when an incorrect vertical structure is used in the retrieval algorithm.

Under typical atmospheric conditions,⁴ ~22% of the Rayleigh scattering resides in a layer between 0 and 2 km, whereas most of the aerosols are below 2 km. For this to be simulated, radiance pseudodata have been created by employing a new two-layer model, in which the top layer has 78% of τ_r and $\tau_a = 0.1$, while the bottom layer has 22% of τ_r and $\tau_a = 0.2$. Figure 10 presents two retrievals that use the pseudoradiance data calculated for this new two-layer model. One retrieval assumes the correct vertical structure [Fig. 10(a)], while the other still assumes that all the Rayleigh scattering is above the aerosol [Fig. 10(b)]. The aerosol model is M99 and $\lambda = 865$ nm. The retrieval presented by Fig. 10(a) is just as good as that in Fig. 2(a). This indicates that the inversion technique is capable of retrieving excellent values of ω_0 and $P(\Theta)$ under this more realistic situation in which the correct vertical structure is used. From Fig. 10(b), we can see that an incorrect assump-

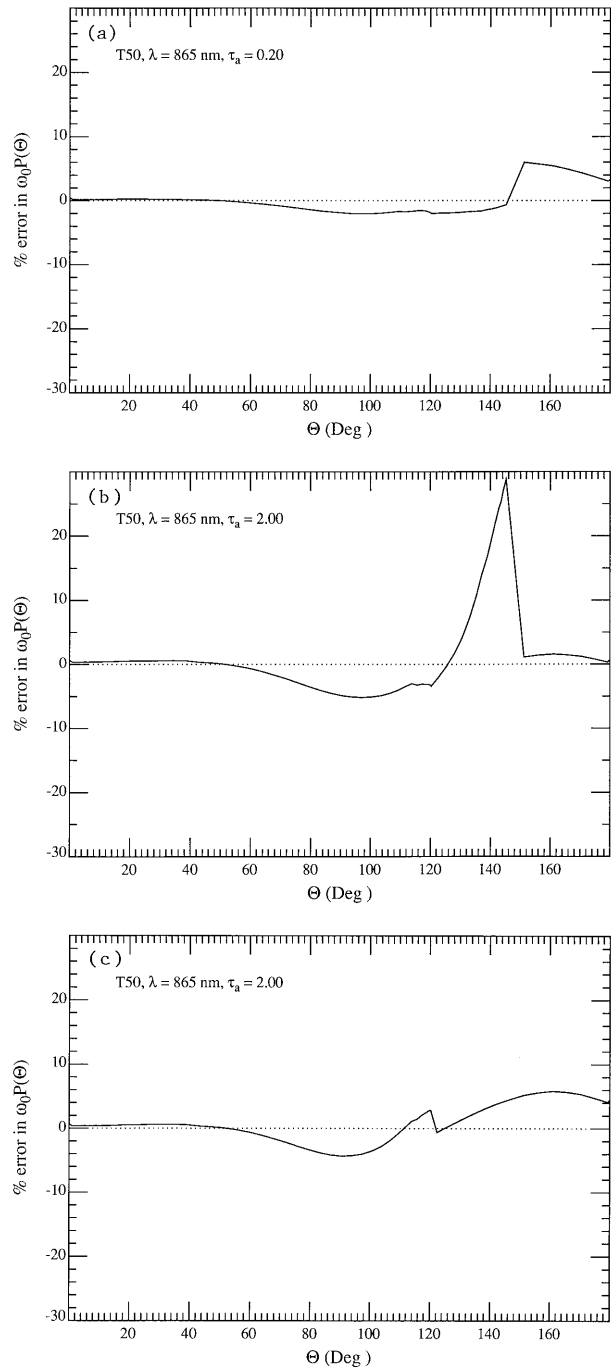


Fig. 9. Percent error in the retrieved $\omega_0 P(\Theta)$ for T50 aerosol when $\rho_B^{(m)}$ and $\rho_T^{(m)}$ are computed by using the vector radiative transfer theory, with $\theta_0 = 60^\circ$ and $\lambda = 865$ nm: (a) $\tau_a = 0.2$; (b) $\tau_a = 2.0$; (c) $\tau_a = 2.0$, but the downwelling principal plane data were replaced by upwelling data.

tion for the vertical structure of the atmosphere does not degrade the retrieval seriously when the retrieval is carried out at $\lambda = 865$ nm. The maximum error in $\omega_0 P(\Theta)$ is ~12% and the error in the retrieved ω_0 is ~0.1%. Computations similar to those presented in Fig. 10 but with an aerosol optical thickness of 1.33 in the lower layer and 0.67 in the upper layer (total $\tau_a = 2.0$) yielded similar results. Figure 11 provides sim-

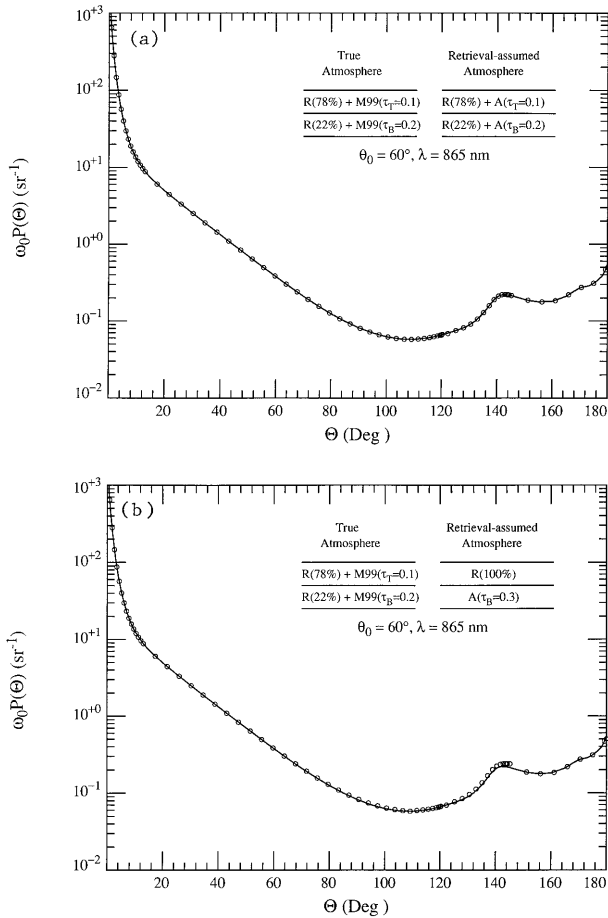


Fig. 10. Comparison between the true $\omega_0 P(\theta)$ (solid curve) and the retrieved $\omega_0 P(\theta)$ for M99 aerosol when Rayleigh scattering and aerosol scattering are mixed in both layers, with $\theta_0 = 60^\circ$ and $\lambda = 865$ nm: (a) retrieval code uses the correct vertical structure in τ_α ; (b) retrieval code uses an incorrect vertical structure.

ilar retrievals for $\lambda = 412$ nm. Again, when the correct vertical structure can be determined and used in the retrieval algorithm, the results are excellent [Fig. 11(a)]. In contrast to the retrieval carried out at 865 nm, an incorrect assumption for the vertical structure results in a very large error in the retrieved $\omega_0 P(\theta)$ at $\lambda = 412$ nm, with the maximum being $\sim 125\%$. However, the retrieval of ω_0 is still excellent: the error is $< 0.5\%$. Replacing the downwelling principal plane data with upwelling data in this case reduces the maximum error in $\omega_0 P(\theta)$ to $\sim 70\%$, and the error in ω_0 to negligible values. These simulations suggest that an incorrect assumption for the vertical structure does not affect the retrieval results seriously at $\lambda = 865$ nm, but at $\lambda = 412$ nm it will cause a large error in the retrieved phase function.

The results presented in Fig. 10 and 11 apply when there is only one type of aerosol involved, e.g., M99. However, the aerosol particles in the boundary layer near the ocean surface are usually larger and contain more condensed water vapor, whereas the particulates suspended within the troposphere above the

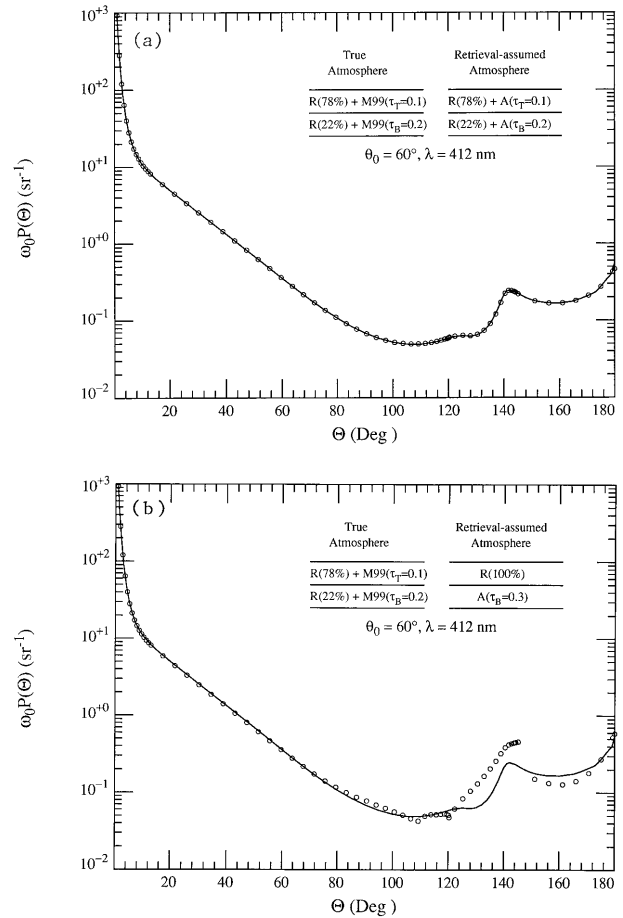


Fig. 11. Same as Fig. 10, except $\lambda = 412$ nm.

boundary layer are smaller and dryer. Therefore, a more realistic two-layer model has been established: the top layer consists of 78% of Rayleigh-scattering molecules and T50 aerosols with $\tau_\alpha = 0.1$, while the bottom layer contains 22% of molecules and M99 aerosols with $\tau_\alpha = 0.2$. When the simulations presented in Fig. 12 are carried out, the pseudoradiance data were created by applying this new two-layer model. For the retrieval presented in Fig. 12(a), the correct vertical structure was assumed; however, in the absence of information regarding the aerosol type, the aerosols in both layers were assumed to be the same. As expected, most of the retrieved $\omega_0 P(\theta)$ (circles) fall between the two dashed curves [which are the true values of $\omega_0 P(\theta)$ for M99 and T50]. Furthermore, for most scattering angles, the circles are very close to the solid curve, which is the effective $\omega_0 P(\theta)$ for the atmospheric column, expressed by

$$[\omega_0 P(\theta)]_{\text{effective}} = \frac{[\omega_0 P(\theta)]_T \tau_T + [\omega_0 P(\theta)]_B \tau_B}{\tau_T + \tau_B}, \quad (15)$$

where T and B indicate aerosol properties in the top and bottom layer, respectively. The retrieved ω_0 is close (within $\sim 0.2\%$) to the effective ω_0 :

$$[\omega_0]_{\text{effective}} = \frac{[\omega_0]_T \tau_T + [\omega_0]_B \tau_B}{\tau_T + \tau_B}, \quad (16)$$

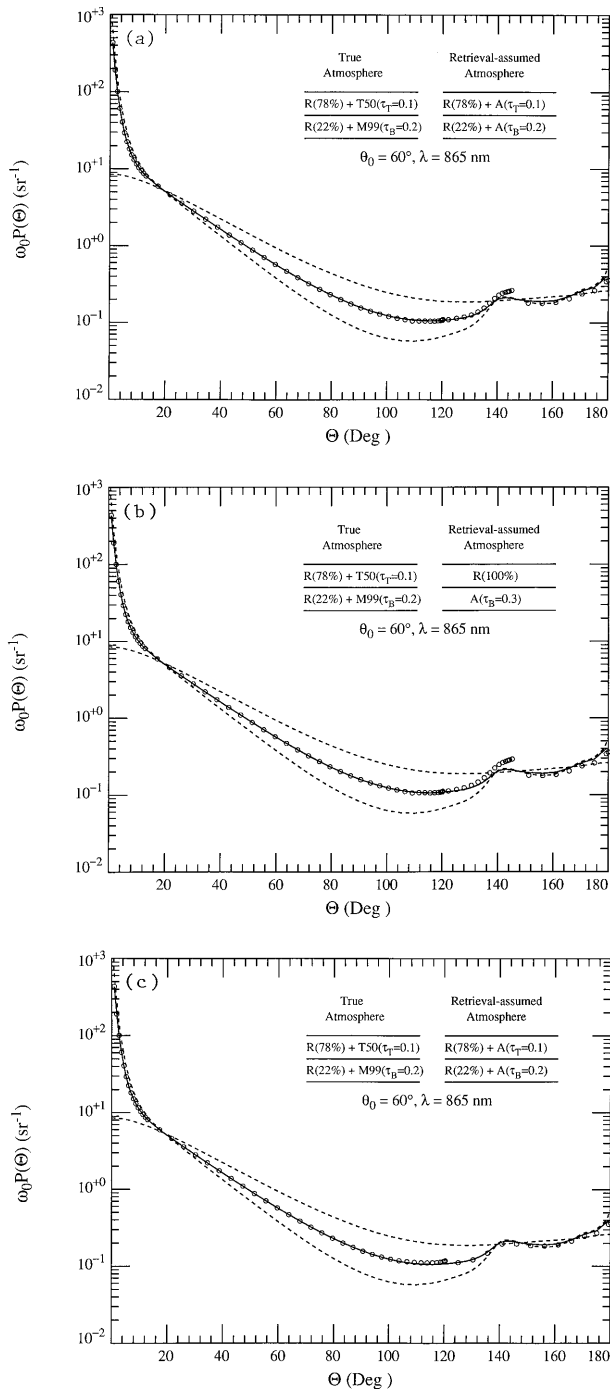


Fig. 12. Comparison between the true $\omega_0 P(\Theta)$ (dashed curves), the retrieved $\omega_0 P(\Theta)$ (circles), and the averaged $\omega_0 P(\Theta)$ (solid curve) for the vertical structure described in the text, with $\theta_0 = 60^\circ$ and $\lambda = 865 \text{ nm}$: (a) correct vertical structure; (b) incorrect vertical structure; (c) same as (a) except that the downwelling principal plane data were replaced by upwelling data.

where $[\omega_0]_T$ and $[\omega_0]_B$ are the values of ω_0 in the top and bottom layers, respectively. The retrieval presented by Fig. 12(b) uses an incorrect assumption for the vertical structure—Rayleigh scattering all above aerosol. Comparing this figure with Fig. 12(a), we see that the incorrect assumption for the vertical structure did not significantly affect the retrieval.

We also notice that, in both figures, the large differences between circles and the solid curve always happen within the range $120^\circ < \Theta < 150^\circ$, where $\omega_0 P(\Theta)$ are retrieved from downwelling principal plane data. Figure 12(c) presents the results of a retrieval as in Fig. 12(a) but uses upwelling radiance data to retrieve $\omega_0 P(\Theta)$ for $120^\circ < \Theta < 150^\circ$. The error between the retrieved and the averaged $\omega_0 P(\Theta)$ is significantly reduced.

Computations similar to those in Fig. 12(a) and 12(b) were carried out with an M99 optical thickness of 1.33 in the lower layer and a T50 optical thickness of 0.67 in the upper layer. The retrieved values of ω_0 were unchanged, but the aerosol phase function showed larger errors for $\Theta \geq 100^\circ$. Also, nearly identical results were obtained with the incorrect and correct vertical structures. Retrievals similar to those presented in Fig. 12, but for $\lambda = 412 \text{ nm}$, have also been carried out. The results show similar patterns except that for backward scattering ($\Theta > 100^\circ$), the errors between the retrieved and the averaged $\omega_0 P(\Theta)$ are much larger than those at $\lambda = 865 \text{ nm}$.

Neither M99 aerosol nor T50 aerosol has strong absorption, i.e., $\omega_0 > 0.92$. To investigate the algorithm's performance when an incorrect assumption is made for the vertical structure involving strongly absorbing aerosols, we have carried out simulations similar to those presented by Figs. 10–12, replacing the M99 aerosol model by the Shettle and Fenn⁶ urban aerosol model with a relative humidity of 50% (U50), for which $\omega_0 = 0.603$ at 865 nm. The results are similar to the M99–T50 cases, indicating that strong aerosol absorption does not degrade the algorithm's performance.

When there are different aerosol types in the top and bottom layers (as in Fig. 12), the current algorithm can retrieve only the effective phase function and the effective single-scattering albedo. Simulations by application of a modified algorithm show that, if somehow the aerosol properties of one of the two layers are available, the phase function and single-scattering albedo of the other one can be retrieved.

4. Concluding Remarks

Here an iterative multiple-scattering retrieval algorithm for inverting the radiances exiting the top and bottom of the atmosphere over a flat ocean to yield the columnar aerosol optical properties [ω_0 and $P(\Theta)$] has been presented. In this algorithm, the single-scattering approximation is used only to indicate the direction (increasing or decreasing) and an approximate amount to vary $\omega_0 P(\Theta)$ at each step of the iteration. As all significant orders of multiple scattering are taken into account, the algorithm is capable of retrieving ω_0 and $P(\Theta)$ for a large aerosol optical thickness. Simulations show that this inversion method, when combined with surface and aircraft (or satellite) measurements, has the potential to retrieve accurate aerosol optical properties over oceans and large lakes, where the surface albedo is low and nearly uniform. The focus of this study was

Table 1. Error in retrieved ω_0 at $\lambda = 865$ nm (M99)^a

Error (%) or Assumption	$\tau_a = 0.2$	$\tau_a = 2.0$
τ_a : ± 5	∓ 3	± 0.1 – 0.5
ρ_T, ρ_B : $\pm 5, \pm 5$	± 4	± 1
ρ_T, ρ_B : $\pm 5, \mp 5$	∓ 4	∓ 1
Noise in ρ_T, ρ_B : 0.5	~ 0.2	~ 0.1
Surface roughness	~ 0.1	~ 0.1
Earth's curvature	~ 0.4	~ 0.1
Polarization	~ 0.1	~ 0.1
Vertical structure		
correct	~ 0.2	~ 0.1
incorrect	~ 0.2	~ 0.1

^aThe error is due to a measurement error or to incorrect assumptions used in the inversion algorithm.

to examine the performance of the algorithm in realistic situations, e.g., when there is error or noise in the measured radiances.

The study of the algorithm's sensitivity to radiometric calibration errors indicates that the retrieved ω_0 is surprisingly stable for a large aerosol optical thickness (the error being $\sim 1\%$ for 5% errors in ρ_T and ρ_B), and that, in agreement with a single-scattering analysis, the relative error in ω_0 is similar to that in ρ_B for small values of τ_a . In contrast, the error in the retrieved $P(\Theta)$ depends strongly on the error in the measurements. Mean-zero instrumental noise has a negligible effect on the retrieved ω_0 , but it may result in an extremely noisy retrieved phase function, especially at a large τ_a or in the blue part of the spectrum. Simulations with a rough sea surface corresponding to the wind speed of 7.5 m/s show that the error in ω_0 induced by neglecting the sea-surface roughness is $\leq 1\%$; the errors in the retrieved $P(\Theta)$ are usually acceptably small except for those retrieved from the radiances influenced by significant multiple scattering, i.e., at angles associated with the downwelling principal plane pseudodata. Replacing the surface principal plane data by upwelling data considerably improves the retrieval of $P(\Theta)$. Ignoring the Earth's curvature in the retrieval algorithm does not affect the retrieval seriously at $\lambda = 865$ nm. Even though polarization is ignored, this study shows that ω_0 can always be retrieved accurately, but the error in the retrieved phase function can be as large as $\sim 30\%$ for $\tau_a = 2.0$. The study of the variations in the vertical structure shows that an incorrect assumption for the vertical structure does not make a significant difference in the retrieved ω_0 and $P(\Theta)$ at $\lambda = 865$ nm, but in the blue (412 nm) it can cause an extremely large error ($\sim 100\%$) in the retrieved $P(\Theta)$.

Errors in the retrievals of ω_0 are summarized in Table 1, where it is seen that the contribution from the measurement error (in τ_a , ρ_B , and ρ_T) far exceeds that resulting from the assumptions made in the retrieval, as well as the error in the retrieval algorithm itself. Table 1 shows that, in a rms sense, the error in ω_0 introduced by the last six items in Table 1 is roughly an order of magnitude smaller than the error

introduced by the assumed $\pm 5\%$ measurement error in τ_a , ρ_B , and ρ_T . It should not be surprising that ω_0 can be accurately retrieved, as it is well known that the sky radiance contains information regarding aerosol absorption.¹⁶ The accuracy shown here suggests that this algorithm would be useful for studying the absorption properties of aerosols.

Using more upwelling data to replace the downwelling principal plane data almost always improves the retrieval of ω_0 and $P(\Theta)$. (The results in Table 1 include cases in which this replacement has been made.) This is because the upwelling data are less influenced by multiple scattering. So, when possible, more upwelling data should be used in the retrieval to replace the downwelling principal plane data. The reason that most of the simulations in this paper were carried out with downwelling principal plane data is, practically, downwelling data (measured from the surface) are much easier to obtain than upwelling data (measured by aircraft or satellite); however, this situation will be remedied by the launch of the Polarization and Directionality of Earth Radiation mission¹⁷ in the fall of 1996, and the Multi-Angle Imaging SpectroRadiometer¹⁸ mission in the fall of 1998.

The sensitivity studies at $\lambda = 412$ nm showed that the retrieved phase function was usually poor, suggesting that this inversion algorithm will be applicable to the retrievals in the blue only if more accurate instrument calibration is available and other factors (sea-surface roughness, polarization, and so on) are taken into account.

Finally, we have assumed that the measurements are taken under ideal conditions—a cloud-free horizontally homogeneous atmosphere. Simulating the perturbing effects of clouds and the horizontal variations in aerosol concentration and properties on the measurement of sky radiance is beyond the scope of this study.

We are grateful to the National Aeronautics and Space Administration for support under grant NAGW-273 and contracts NAS5-31363 and NAS5-31734, and to the U. S. Office of Naval Research for support under grant N00014-89-J-1985.

References

1. H. R. Gordon and T. Zhang, "Columnar aerosol properties over oceans by combining surface and aircraft measurements: simulations," *Appl. Opt.* **34**, 5552–5555 (1995).
2. T. Zhang, "Remote sensing of aerosol properties over the ocean by combining surface and aircraft measurements," Ph.D. dissertation (University of Miami, Coral Gables, Fla., 1995).
3. M. Wang and H. R. Gordon, "Retrieval of the columnar aerosol phase function and single scattering albedo from sky radiance over the ocean: simulations," *Appl. Opt.* **32**, 4598–4609 (1993).
4. Y. Sasano and E. V. Browell, "Light scattering characteristics of various aerosol types derived from multiple wavelength lidar observations," *Appl. Opt.* **28**, 1670–1679 (1989).
5. G. W. Kattawar, "A three-parameter analytic phase function for multiple scattering calculations," *J. Quant. Spectrosc. Radiat. Transfer* **15**, 839–849 (1975).
6. E. P. Shettle and R. W. Fenn, "Models for the aerosols of the

- lower atmosphere and the effects of humidity variations on their optical properties," Rep. AFGL-TR-79-0214 (U.S. Air Force Geophysics Laboratory, Hanscomb Air Force Base, Mass., 1979).
7. P. J. Reddy, F. W. Kreiner, J. J. Deluisi, and Y. Kim, "Aerosol optical depths over the Atlantic derived from shipboard sun-photometer observations during the 1988 Global Change Expedition," *Global Biogeochem. Cycles* **4**, 225–240 (1990).
 8. G. K. Korotaev, S. M. Sakerin, A. M. Ignatov, L. L. Stowe, and E. P. McClain, "Sun-photometer observations of aerosol optical thickness over the North Atlantic from a Soviet research vessel for validation of satellite measurements," *J. Atmos. Oceanic Technol.* **10**, 725–735 (1993).
 9. Y. V. Villevalde, A. V. Smirnov, N. T. O'Neill, S. P. Smyshlyaev, and V. V. Yakovlev, "Measurement of aerosol optical depth in the Pacific Ocean and North Atlantic," *J. Geophys. Res.* **99 D**, 20983–20988 (1994).
 10. C. Cox and W. Munk, "Measurements of the roughness of the sea surface from photographs of the Sun's glitter," *J. Opt. Soc. Am.* **44**, 838–850 (1954).
 11. K. Ding, "Radiative transfer in spherical shell atmospheres for correction of ocean color remote sensing," Ph.D. dissertation (University of Miami, Coral Gables, Fla., 1993), 89 pp.
 12. G. W. Kattawar, G. N. Plass, and S. J. Hitzfelder, "Multiple scattered radiation emerging from Rayleigh and continental haze layers. 1: Radiance, polarization, and neutral points," *Appl. Opt.* **15**, 632–647 (1976).
 13. H. R. Gordon, J. W. Brown, and R. H. Evans, "Exact Rayleigh scattering calculations for use with the Nimbus-7 coastal zone color scanner," *Appl. Opt.* **27**, 862–871 (1988).
 14. H. R. Gordon and M. Wang, "Surface roughness considerations for atmospheric correction of ocean color sensors. 1: The Rayleigh scattering component," *Appl. Opt.* **31**, 4247–4260 (1992).
 15. H. R. Gordon and M. Wang, "Surface roughness considerations for atmospheric correction of ocean color sensors. 2: Error in the retrieved water-leaving radiance," *Appl. Opt.* **31**, 4261–4267 (1992).
 16. M. D. King and B. M. Herman, "Determination of the ground albedo and the index of absorption of atmospheric particulates by remote sensing. Part I: Theory," *J. Atmos. Sci.* **36**, 163–173 (1979).
 17. P. Y. Deschamps, F. M. Bréon, M. Leroy, A. Podaire, A. Bricaud, J. C. Buriez, and G. Sèze, "The POLDER mission: instrument characteristics and scientific objectives," *IEEE Trans. Geosci. Remote Sensing* **32**, 598–615 (1994).
 18. D. J. Diner, C. J. Bruegge, J. V. Martonchik, T. P. Ackerman, R. Davies, S. A. W. Gerstl, H. R. Gordon, P. J. Sellers, J. Clark, J. A. Daniels, E. D. Danielson, V. G. Duval, K. P. Klaasen, G. W. L. A. D. I. Nakamoto, R. Pagano, and T. H. Reilly, "MISR: a Multi-Angle Imaging SpectroRadiometer for geophysical and climatological research from EOS," *IEEE Trans. Geosci. Remote Sensing* **27**, 200–214 (1989).